JOURNAL OF COMPUTATIONAL PHYSICS 40, 143–166 (1981)

Two-Dimensional Predictor–Corrector Method of Characteristics for Fluid–Structure Interactions

K. TAKEUCHI AND A. C. SPENCER

Westinghouse Electric Corporation, Nuclear Energy Systems, Pittsburgh, Pennsylvania 15230

Received March 25, 1980; revised May 29, 1980

Fluid–structure interactions in a concentric cylinder are incorporated in CHARM, originally a hydraulic code based on a two-dimensional method of characteristics. An initial test calculation illustrates that a small error in the fluid flow distribution created by structural motion results in a significant over-response of the fluid pressure. To improve the accuracy, a predictor–corrector method is developed and it is now incorporated in CHARM. In this method, use is made of the explicit scheme for predictor computation and an implicit scheme for corrector computation. It is found that the corrector computation is important especially to a coarse mesh model.

1. INTRODUCTION

During a hypothetical loss of coolant accident (LOCA), a rarefaction wave created at a pipe break propagates into reactor internals. As the wave reaches the downcomer annulus, the core barrel is subjected to a hydraulic force resulting in mechanical deformation which in turn alters the force field. Such fluid–structure interactions make significant contributions to the hydraulic force exerted to the structure for evaluation of structural integrity [1].

One method widely used in reactor technology for core barrel deformation is the hydrodynamic mass or the virtual mass representation of fluid–structure interactions which is based on invicid, incompressible fluid flow [2–5]. Because of the fluid incompressibility assumption, this method may not be reliable in analyses of a LOCA transient [6]. To improve this shortcoming, recent effort has been made to develop the more fundamental approach, that is, to solve explicitly both structural dynamic equations and hydraulic conservation equations, simultaneously [7–10]. For example, the MULTIFLEX code solves one-dimensional hydraulic conservation equations by the method of characteristics and the structural dynamic equations by the use of modal analyses or by the direct integration method. It is shown [11] that the code indeed computes correctly not only the hydrodynamic mass but also fluid compression effects and the effect of structural motion of changing the sonic velocity. The last effect, for example, is verified by comparison of MULTIFLEX calculation with the SRI experiment [12] for pressure wave propagation through water contained

0021-9991/81/030143–24$02.00/0

581/40/1-10

in a plastically deforming pipe. The DAPSY(GRS) code [13] is reported to be based on the method similar to MULTIFLEX.

For a multi-dimensional system of fluid–structure interactions, the K-FIX code [8], the combined YAQUIR/CYCLDY2 [9] code, the SOLA-FLEX code [10], and so on have been developed (see Ref. [14] for a brief review of these codes and verifications). All of these multi-dimensional codes solve the hydraulic conservation equations by the finite difference method. An alternative approach is to utilize the method of characteristics for the hydraulic conservation equation modified to include variable boundaries to simulate fluid–structure interactions. Such an approach is taken here for the two-dimensional case, basing the hydraulics on techniques developed for the CHARM code [15]. Namely, fluid–structure interactions have been incorporated in CHARM. A test was conducted with a simple problem in Ref. [8] and a numerical phenomenon unique to fluid–structure interaction system is found as described in the next. Briefly discussed in Section 2 is derivation of characteristic equations with variable boundary perpendicular to the hydraulic flow field. In Section 3.1, explicit difference equations are derived and the method of computation is tested in Section 3.2 with a sample problem whose analytic solution is given in Appendix A. To increase accuracy at coarse mesh spacings, a corrector calculation, discussed in Section 3.3, is applied to the explicit results. Following the suggestion given in Ref. [12], this corrector method is to use the implicit difference equations. Results of study are summarized and discussed in Section 4.

2. Two-Dimensional Method of Characteristics with Variable Fluid Thickness

In a PWR downcomer annulus, the hydraulic conservation equations can be reasonably described in a cartesian coordinate system (x, y): the x-axis for a circumferential direction and the y-axis for the axial direction. The fluid state is described by the pressure p, the density ρ, and the x- and y-direction fluid velocities u and v, respectively. Due to the relative motion of the barrel and the vessel, the gap D of the annulus varies with time. For this system the hydraulic conservation equations become:

Mass Conservation,

$$\frac{\partial \rho}{\partial t} + u\frac{\partial \rho}{\partial x} + v\frac{\partial \rho}{\partial y} + \rho\frac{\partial u}{\partial x} + \rho\frac{\partial v}{\partial y} = -\rho\Gamma\frac{\dot{D}}{D}; \tag{1}$$

Momentum Conservation,

$$\rho\left(\frac{\partial u}{\partial t} + u\frac{\partial u}{\partial x} + v\frac{\partial u}{\partial y}\right) + \frac{\partial p}{\partial x} = \rho F_x, \tag{2}$$

$$\rho\left(\frac{\partial v}{\partial t} + u\frac{\partial v}{\partial x} + v\frac{\partial v}{\partial y}\right) + \frac{\partial p}{\partial y} = \rho F_y; \tag{3}$$

Energy Conservation,

$$-c^2\left(\frac{\partial \rho}{\partial t}+u\frac{\partial \rho}{\partial x}+v\frac{\partial \rho}{\partial y}\right)+\left(\frac{\partial p}{\partial t}+u\frac{\partial p}{\partial x}+v\frac{\partial p}{\partial y}\right)=0, \tag{4}$$

where c is the sonic velocity and spatial derivatives of the gap thickness D have been ignored because these magnitudes are on the order of u/c or v/c relative to the time derivative $\dot{D}$. Factor Γ in Eq. (1) is a geometrical contribution, $\Gamma = 2R_B/(R_B + R_V)$, to the volume change of annulus made by motion of the inner cylinder, where R_B and R_V are the inner and outer radii of the annulus.

In order to derive characteristic equations, the above equations are written in a matrix form for a column vector $U \equiv \{\rho u v p\}$,

$$M_t\frac{\partial U}{\partial t}+M_x\frac{\partial U}{\partial x}+M_y\frac{\partial U}{\partial y}=S, \tag{5.1}$$

where

$$Mt \equiv \begin{Bmatrix} 1 & 0 & 0 & 0 \\ 0 & \rho & 0 & 0 \\ 0 & 0 & \rho & 0 \\ -c^2 & 0 & 0 & 1 \end{Bmatrix}, \tag{5.2}$$

$$M_x \equiv \begin{Bmatrix} u & \rho & 0 & 0 \\ 0 & \rho u & 0 & 1 \\ 0 & 0 & \rho u & 0 \\ -c^2 u & 0 & 0 & u \end{Bmatrix}, \tag{5.3}$$

$$M_y \equiv \begin{Bmatrix} v & 0 & \rho & 0 \\ 0 & \rho v & 0 & 1 \\ 0 & 0 & \rho v & 0 \\ -c^2 v & 0 & 0 & v \end{Bmatrix}, \tag{5.4}$$

$$S \equiv \begin{Bmatrix} -\rho\Gamma\dot{D}/D \\ \rho F_x \\ \rho F_y \\ 0 \end{Bmatrix}. \tag{5.5}$$

Then, Eq. (5.1) is transformed by a row vector $A^T = (a_1 a_2 a_3 a_4)$,

$$A^T M_t\frac{\partial U}{\partial t}+A^T M_x\frac{\partial U}{\partial x}+A^T M_y\frac{\partial U}{\partial y}=A^T S. \tag{6}$$

The condition for the characteristic is given by the eigenvalue problem,

$$(\lambda_t M_t^T+\lambda_x M_x^T+\lambda_y M_y^T)A=0, \tag{7}$$

where

$$\sum \lambda_i M_i^T = \begin{pmatrix} f & 0 & 0 & -c^2 f \\ \rho\lambda_x & \rho f & 0 & 0 \\ \rho\lambda_y & 0 & \rho f & 0 \\ 0 & \lambda_x & \lambda_y & f \end{pmatrix} \tag{8.1}$$

and

$$f \equiv \lambda_t + u\lambda_x + v\lambda_y. \tag{8.2}$$

The first solution of the eigenvalue problem is the eigenvalue $f = 0$ and the eigenfunction $A^T = (0001)$ with which Eq. (6) becomes the material characteristic equation

$$\frac{Dp}{Dt_0} = -\rho c^2 \left(\frac{\partial u}{\partial x} + \frac{\partial v}{\partial y}\right) - \rho c^2 \Gamma \frac{\dot{D}}{D}, \tag{9}$$

where

$$\frac{D}{Dt_0} = \frac{\partial}{\partial t} + u\frac{\partial}{\partial x} + v\frac{\partial}{\partial y} \tag{10}$$

and use has been made of Eq. (1) to eliminate derivative of density. The second eigenvalue is continuously infinite $f = \lambda c$ specified by a parameter α, $\lambda_x = \lambda \cos\alpha$ and $\lambda_y = \lambda \sin\alpha$. The corresponding eigenvector is $A^T = (c^2 \; -\rho c \cos\alpha \; -\rho c \sin\alpha \; 1)$. Then, Eq. (6) becomes the sonic characteristic equation,

$$\begin{aligned} &\frac{Dp}{Dt} - \rho c \cos\alpha \frac{Du}{Dt} - \rho c \sin\alpha \frac{Dv}{Dt} + \rho c^2(1 - \cos^2\alpha)\frac{\partial u}{\partial x} \\ &\qquad - \rho c^2 \sin\alpha \cos\alpha \frac{\partial u}{\partial y} - \rho c^2 \sin\alpha \cos\alpha \frac{\partial v}{\partial x} + \rho c^2(1 - \sin^2\alpha)\frac{\partial v}{\partial y} \\ &= -\rho c^2 \Gamma \frac{\dot{D}}{D} - \rho c F_x \cos\alpha - \rho c F_y \sin\alpha, \end{aligned} \tag{11}$$

where

$$\frac{D}{Dt} \equiv \frac{\partial}{\partial t} + (u - c\cos\alpha)\frac{\partial}{\partial x} + (v - c\sin\alpha)\frac{\partial}{\partial y}. \tag{12}$$

Equation (9) is the material characteristic equation and Eq. (11) is a continuously infinite number of sonic characteristic equations as specified by variable α. For the purpose of numerical computation, four sonic equations are selected with $\alpha = 0$, $\pi/2$, π, and $3\pi/2$. These equations are integrated along respective characteristics, Eqs (10) and (12), to derive explicit and implicit difference equations.

These characteristics in space–time coordinate system (x, y, t) are illustrated in Fig. 1 for an explicit numerical scheme; the x–y plane in this figure is drawn at a time

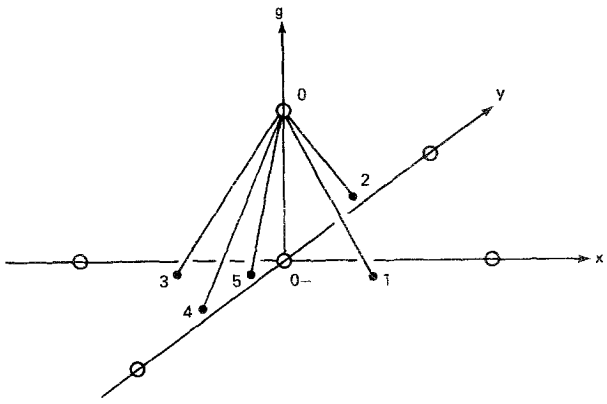

FIG. 1. Characteristics for explicit scheme.

when the hydraulic quantities are known at the nodes indicated by open circles. Open circle 0 is the node at the present time step where the hydraulic quantities must be computed. In this situation, the characteristic lines intersecting point 0 intersect the x–y plane at closed circles 1–5 for u, $v > 0$. Line $\overline{05}$ is the material characteristics and lines $\overline{01}$, $\overline{02}$, $\overline{03}$, and $\overline{04}$ are the sonic characteristics with $\alpha = 0$, $\pi/2$, π, and $3\pi/2$, respectively.

The characteristic lines for the implicit scheme are illustrated in Fig. 2. In this case, the x–y plane is shown at the current time step of interest and the characteristic lines originates at point 0– at the previous time step. These lines intersect the x–y plane at points 1+ through 5+. Line $\overline{0-5+}$ is the material characteristics and lines $\overline{0-1+}$, $\overline{0-2+}$, $\overline{0-3+}$, and $\overline{0-5+}$ are the sonic characteristics with $\alpha = 0$, $\pi/2$, π and $3\pi/2$, respectively.

The explicit and implicit difference equations are discussed in the next section; The explicit difference equations are used as a predictor computation and the implicit difference equations as a corrector computation.

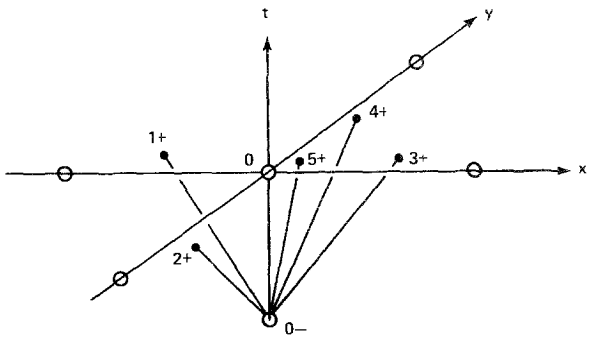

FIG. 2. Characteristics for implicit scheme.

3. Difference Equations and Results of Sample Computations

The characteristic equations obtained in the previous section are integrated along their respective characteristics to derive difference equations. The obtained difference equations are shown in Section 3.1 for an explicit scheme and computation procedures are briefly described. To test the method of computation, a sample problem is solved in Section 3.2 and the results are compared with the analytic solution in Appendix A. In order to improve the computation, implicit difference equations are used for corrector computation discussed in Section 3.3.

3.1. *Explicit Difference Equations for Predictor Computations*

Explicit difference equations are obtained by integrating the characteristic equation along the explicit characteristic lines in Fig. 1 with the source term evaluated at the previous time step. For example, the material characteristic equation (9) is integrated along line $\overline{50}$ and the obtained difference equation is

$$p_0 = P_5 - \rho c^2 \Gamma \frac{\Delta D}{D}, \tag{13}$$

where

$$P_5 \equiv p_5 - \Delta t \, \mathscr{G}_5 \tag{14.1}$$

and

$$\mathscr{G}_5 \equiv \rho c^2 \left(\frac{\partial u}{\partial x} + \frac{\partial v}{\partial y} \right). \tag{14.2}$$

The quantities with subscripts 0 and 5 are those at the points 0 and 5 in Fig. 1. ΔD is increment of the annulus gap in time step Δt. Similarly, the sonic difference equations are obtained as follows;

$\alpha = 0$ characteristic equation,

$$p_0 - \rho c u_0 = P_1 - \rho c^2 \Gamma \frac{\Delta D}{D}, \tag{15}$$

where

$$P_1 \equiv p_1 - \rho c u_1 - \Delta t \, \mathscr{G}_1, \tag{16.1}$$

$$\mathscr{G}_1 \equiv \rho c F_x + \rho c^2 \frac{\partial v}{\partial y}; \tag{16.2}$$

$\alpha = \pi/2$ characteristic equation,

$$p_0 - \rho c v_0 = P_2 - \rho c^2 \Gamma \frac{\Delta D}{D}, \tag{17}$$

where

$$P_2 \equiv p_2 - \rho c v_0 - \Delta t\, \mathscr{G}_2, \tag{18.1}$$

$$\mathscr{G}_2 \equiv \rho c F_y + \rho c^2 \frac{\partial u}{\partial x}$$

$\alpha = \pi$ characteristic equation,

$$p_0 + \rho c u_0 = P_3 - \rho c^2 \Gamma \frac{\Delta D}{D}, \tag{19}$$

where

$$P_3 \equiv p_3 + \rho c u_3 - \Delta t\, \mathscr{G}_3, \tag{20.1}$$

$$\mathscr{G}_3 \equiv -\rho c F_x + \rho c^2 \frac{\partial v}{\partial y}. \tag{20.2}$$

$\alpha = 3\pi/2$ characteristic equation,

$$p_0 + \rho c v_0 = P_4 - \rho c^2 \Gamma \frac{\Delta D}{D}, \tag{21}$$

where

$$P_4 \equiv p_4 + \rho c v_4 - \Delta t\, \mathscr{G}_4, \tag{22.1}$$

$$\mathscr{G}_4 \equiv -\rho c F_y + \rho c^2 \frac{\partial u}{\partial x}. \tag{22.2}$$

The expression for circumferential velocity u_0 is obtained by difference of Eqs. (15)

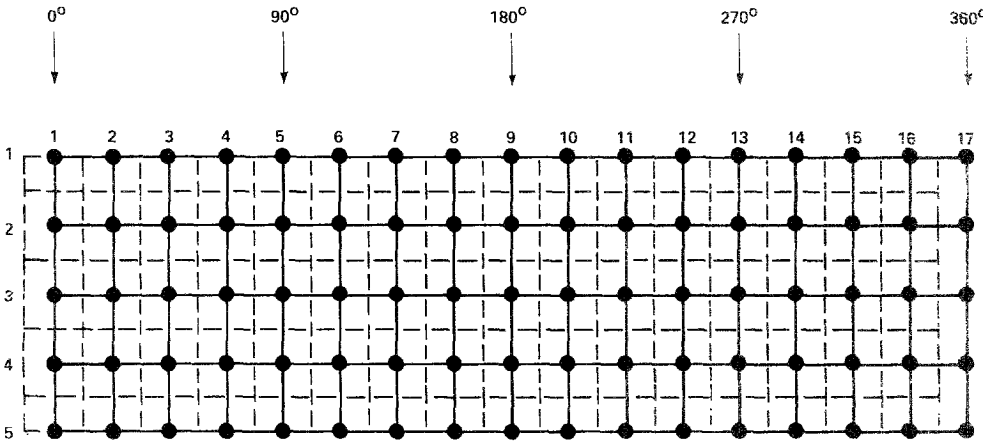

FIG. 3. Modeling of an infinite annulus with fluid/structure interfacing, (16 × 5) node model.

and (19) and similarly v_0 is computed from Eqs. (17) and (21). Pressure p_0 is derived by a linear combination of Eqs. (13), (15), (17), and (21).

The obtained expressions for u_0 and v_0 do not have the term of fluid structure interaction $\Delta D/D$, while the expression for p_0 does. Therefore, immediate response to the structural deformation is variation of the pressure field but not u_0 and v_0. These velocity fields may be influenced later on via pressure field variation.

Increment of the annulus gap, ΔD, at a hydraulic node n is actually structural deformation, $-\Delta X_i$, of the structural wall i interfacing the hydraulic node. The structural deformation, vector $[X]$, is determined by the equation of structural motion,

$$\{M\}[\ddot{X}] + \{K\}[X] = [f(p)], \tag{23}$$

subjected to the hydraulic force on the right-hand side, where $\{M\}$ and $\{K\}$ are mass and stiffness matrices of the inner cylinder, respectively. The hydraulic force $f_i(p)$ acting on the wall i is the wall area times pressure differential across the wall, W_i $(p_{\text{ref}} - p_n)$. This hydraulic force and $\Gamma \Delta D/D$ in Eqs. (13), (15), (17), (19), and (21)

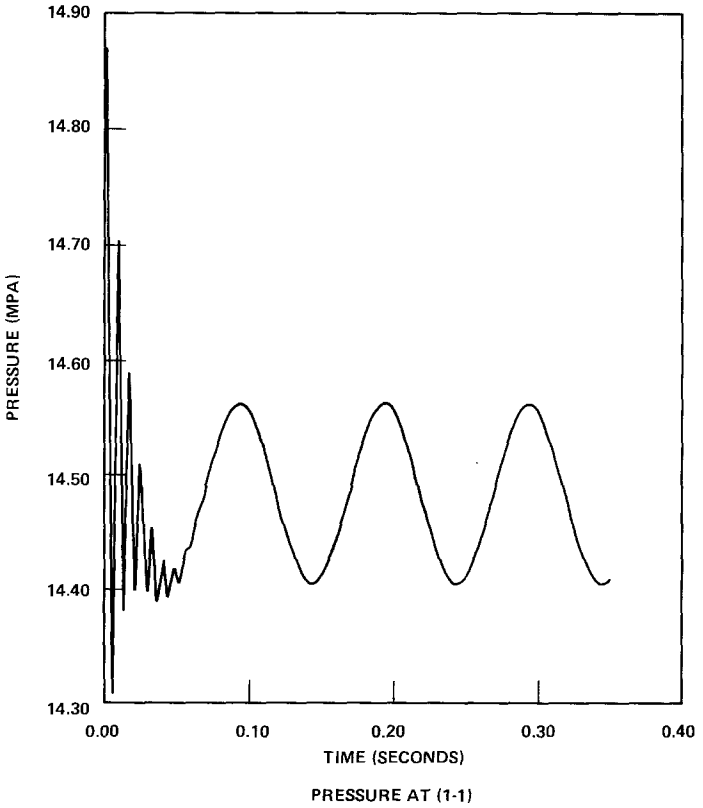

FIG. 4. Pressure history at $x = 0$ of (16×5) node model, explicit computation.

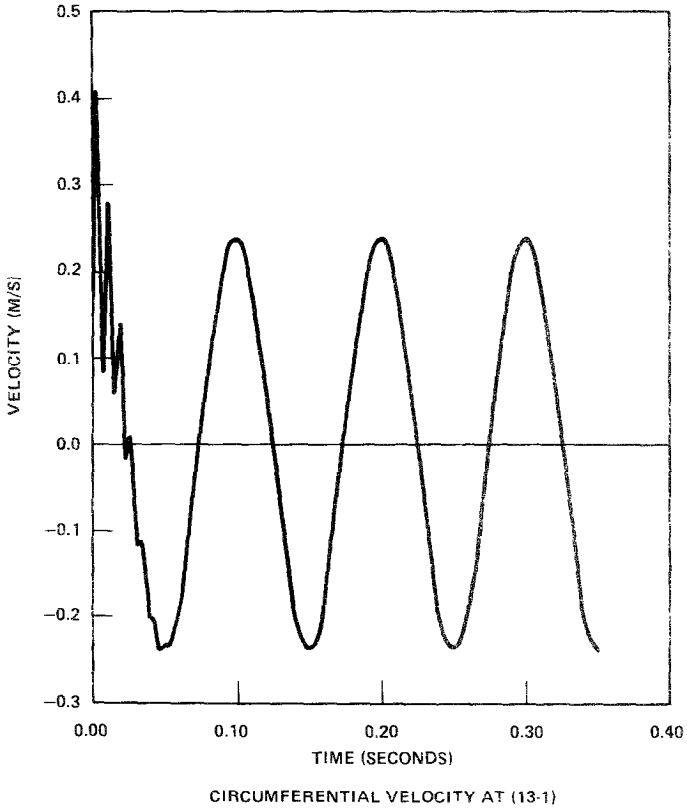

FIG. 5. Velocity history at $x = L/4$ of (16×5) node model, explicit computation.

constitute the coupling between the hydraulic and structural systems and these equations and Eq. (23) are solved simultaneously. In the following sample problem, however, ΔD is given as a forcing function and so Eq. (23) will not be solved. This specification of ΔD precludes any interaction of the fluid back on the structure through the hydraulic force $f(p)$ so that communication is in one direction only.

In numerical computation, time step is chosen such that the hydraulic solution without fluid structure interactions is stable. Such a condition is discussed in Ref. [15],

$$\Delta t < \min_{i,j} \frac{1}{\dfrac{c+|u|}{\Delta x} + \dfrac{c+|v|}{\Delta y}}, \tag{24}$$

where min is the minimum value at all the nodes (i,j) in the grids made of circumferential spacing Δx and axial spacing Δy.

3.2. *A Sample Problem*

To test the method of computation, consider an infinite concentric cylinder with $R_B = 1.829$ m and $R_V = 2.073$ m filled with water of density $\rho = 977.7$ kg/m^3 and the sonic velocity $c = 1570.$ m/s under an initial pressure $p_0 = 14.485$ MPa. A transient is created by a sinusoidal oscillation of the inner cylinder with an amplitude $A = 0.508$ mm and a frequency 10 Hz, $\omega_0 = 20\pi$,

$$\begin{aligned} D &= D_0 && \text{for} \quad t < 0 \\ &= D_0 - A \cos 2\pi x/L \sin \omega_0 t && \text{for} \quad t \geqslant 0 \end{aligned} \tag{25}$$

An analytic soution to this problem is obtained in Appendix A by solving a wave equation for the velocity potential. Then, the pressure and the fluid velocity are calculated,

$$p - p_0 = \{a_1 \sin k_0 t - a_2 \sin(\omega_0 t + \phi_p)\} \cos \frac{2\pi x}{L} \tag{26}$$

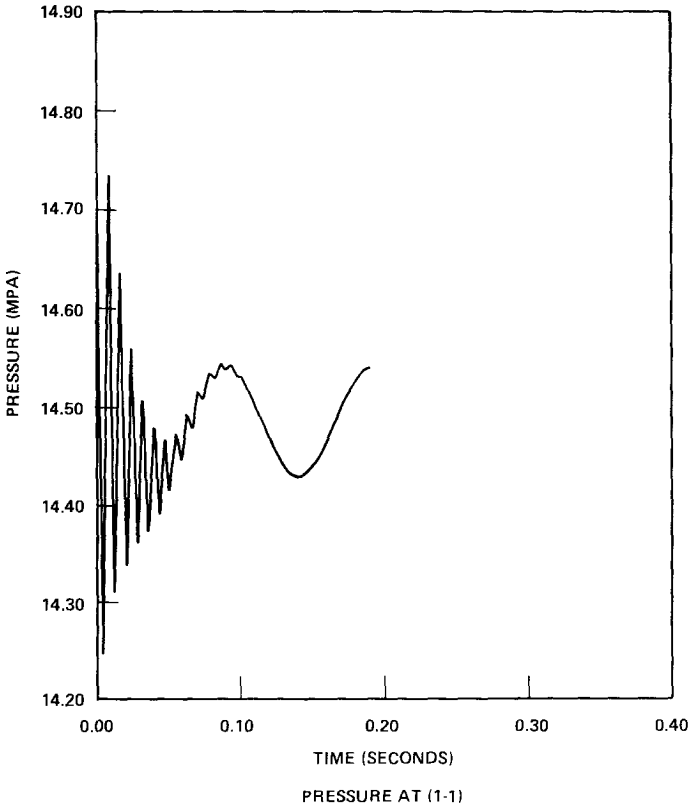

FIG. 6. Pressure history at $x = 0$ of (24×11) node model, explicit computation.

and

$$u = \{-b_1 \cos k_0 t + b_2 \cos(\omega_0 t + \phi_u)\} \sin \frac{2\pi x}{L}, \tag{27}$$

where L is the mid-point circumference and the wave vector $k_0 = 2\pi c/L$. The first terms in Eqs. (26) and (27) are the transient response of acoustic wave oscillation with period of sonic circumferential propagation which usually decays with time due to friction loss in practice. In the above solution, there is no decay factor because such a loss is ignored in the wave equation. The second terms in Eqs. (26) and (27) are the stationary oscillations characterized by the frequency of the external forcing function ω_0. The analytic solution is specified by constants

$$\begin{aligned} a_1 &= 0.3876 \quad \text{(MPa)}, \\ a_2 &= 0.0301 \quad \text{(MPa)}, \\ b_1 &= b_2 = 0.251 \quad \text{(m/s)}, \\ \phi_p &= \phi_u = 0. \end{aligned} \tag{28}$$

This result is used to evaluate numerical computations in the following.

The above problem is numerically solved with the explicit scheme discussed in Section 3.1. The cylindrical annulus of an infinite length is represented by (16×5), (24×5), and (48×5) node models, where (16×5) node model for example is composed of 16 circumferential nodes and 5 axial nodes (see Fig. 3). In this figure, the hydraulic annulus is modeled in practice by (17×5) nodes indicated by circles whose nearest neighbors are connected by solid lines. The nodal spacings are circumferentially 0.766 m and axially 0.852 m. The nodes in the 17th collumn are implemented to provide a proper boundary condition to the nodes in the 16th column; i.e., the hydraulic information in Column 17 is set equal to that in Column 1. The boundary condition in the 1st and the 5th rows is that no axial flow is allowed, $u = 0$. The nodes in the 1st through the 16th columns interface with structural wall segments indicated by dashed lines.

Initially, the fluid is motionless under a uniform pressure, 14.485 MPa. A transient is created by a given structural motion, Eq. (25). During the transient, a constant sonic velocity is maintained, $c = 1570$ m/s.

Figures 4–9 illustrate the computed time histories of the pressure at $x = 0$ and the fluid velocity at $x = L/4$ computed by the 16-, 24-, and 48-node models.

It is generally observed that the acoustic transient of fast oscillation damps quickly and then a steady oscillation remains. The acoustic oscillation is caused by the pressure wave propagation around the circumstance. In fact, its frequency ($c/L = 121$ Hz) agrees very well with the computed frequency of the fast oscillation. The damping of the acoustic transient is due to the numerical dissipation (see Ref. [15]) and the damping rate decreases with the smaller node spacing. In the following stationary transient, the time history of fluid velocity is independent of the node

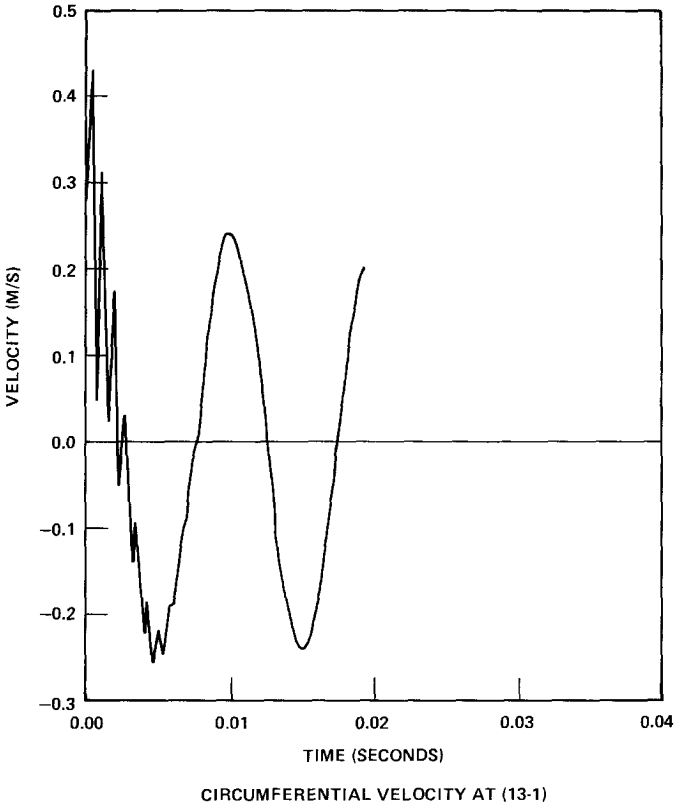

FIG. 7. Velocity history at $x = L/4$ of (24 × 11) node model, explicit computation.

spacing. However, the amplitude and the phase shift of pressure oscillation becomes smaller and in better agreement with the analytic solution, as the spacing decreases. The results are summarized in Table I in terms of constants in Eqs. (26) and (27).

The major error appears in stationary pressure oscillation. This may be attributed to delayed fluid diffusion as is seen by the following discussion. In the analytic

TABLE I

Coefficients in Eqs. (26) and (27) Due to Explicit Computation

Models	Pressure term			Velocity term		
	a_1 (MPa)	a_2 (MPa)	ϕ_p (rad)	b_1 (m/s)	b_2 (m/s)	ϕ_u (rad)
Analytic solution	0.370	0.0288	0.	0.241	0.241	0.
(16 × 5) model	0.469	0.0793	-0.33π	0.244	0.238	0.
(24 × 5) model	0.417	0.0565	-0.33π	0.244	0.239	0.
(48 × 5) model	0.376	0.0370	-0.22π	0.259	0.241	0.

solution shown in Appendix A, time derivative of pressure field can be related to structural deformation and fluid diffusion,

$$\frac{\partial p}{\partial t} = -\rho c^2 \Gamma \frac{\dot{D}}{D_0} - \rho c^2 \frac{\partial u}{\partial x}. \tag{29}$$

Suppose that $\dot{D}$ is the exact value given by Eq. (25) but the fluid velocity is delayed by a phase factor γ from the exact solution. Then, Eq. (26) becomes

$$\begin{aligned}\frac{\partial p}{\partial t} &= \frac{A\rho c^2 \Gamma}{D_0}\left\{\omega_0 \cos \omega_0 t - \frac{k_0^2 \omega_0}{k_0^2 - \omega_0^2}\cos(\omega_0 t - \gamma)\right\}\cos\frac{2\pi}{L}x \\ &\cong \frac{A\rho c^2 \Gamma}{D_0}\left\{-\frac{\omega_0^3}{k_0^2 - \omega_0^2}\cos\omega_0 t - \frac{\gamma k_0^2 \omega_0}{k_0^2 - \omega_0^2}\sin\omega_0 t\right\}\cos\frac{2\pi}{L}x,\end{aligned} \tag{30}$$

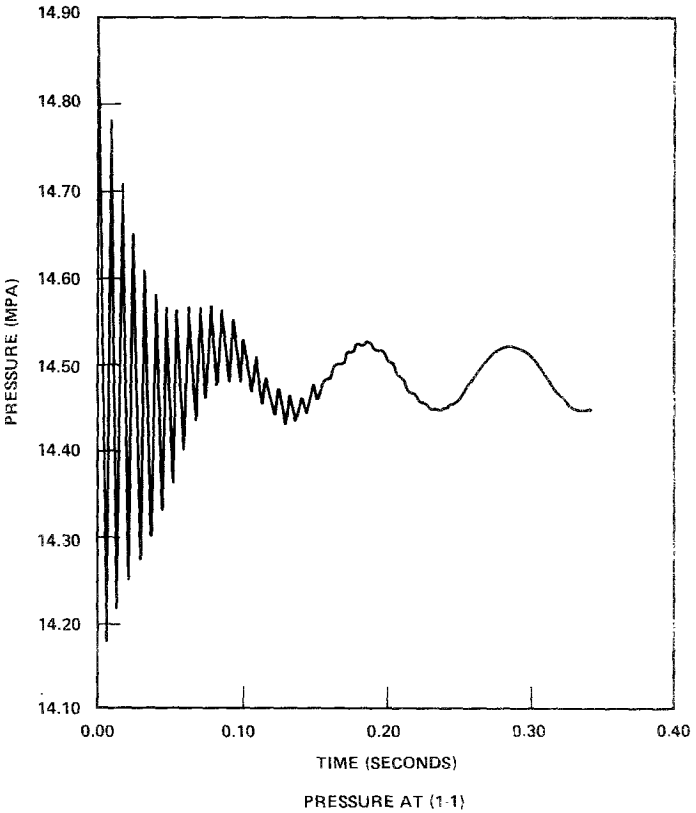

FIG. 8. Pressure history at $x = 0$ of (48×5) node model, explicit computation.

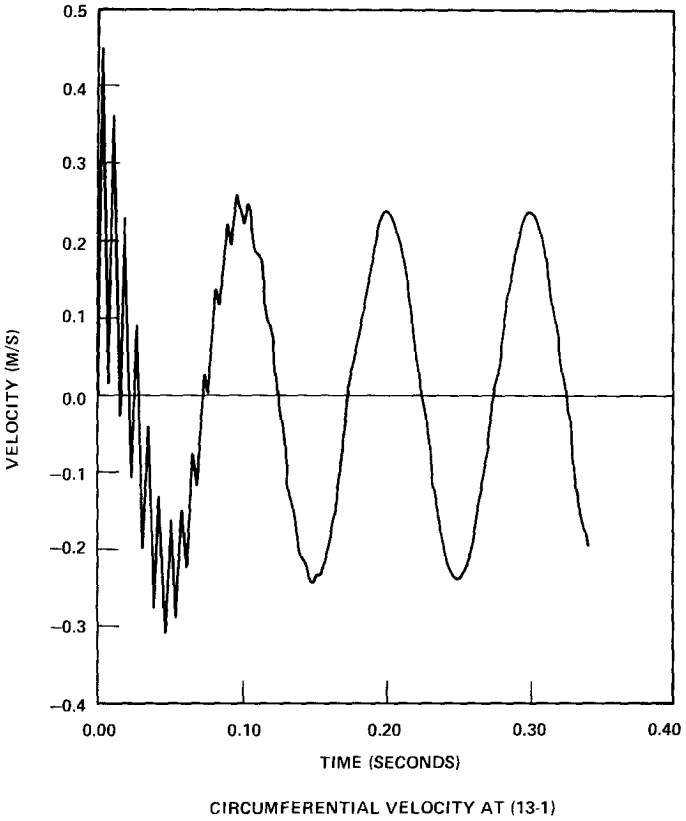

FIG. 9. Velocity history at $x = L/4$ of (48×5) node model, explicit computation.

where $\gamma \ll 1$ is assumed. The solution of this equation is

$$p - p_0 = -\frac{A\rho c^2 \omega_0^2 \Gamma}{k_0^2 - \omega_0^2} \left(1 + \left(\gamma \frac{k_0^2}{\omega_0^2}\right)^2\right)^{1/2} \sin(\omega_0 t - \delta) \cos \frac{2\pi}{L} x, \tag{31}$$

where

$$\tan \delta = \gamma \frac{k_0^2}{\omega_0^2}. \tag{32}$$

Now that $(k_0/\omega_0)^2 = 164$ in the sample problem, the value of γ that makes the amplitude of the pressure oscillation twice as large as the exact solution can be obtained;

$$\gamma = 0.0106 \ (\ll 1),$$

which is equivalent to the delay time $\tau = \gamma/\omega_0 = 0.17$ ms. The phase δ is also calculated; $\delta = 0.33\pi$. Namely, slight delay 0.17 ms (on the order of one time step of (24 × 5) node model computation) in fluid diffusion creates the amplitude of pressure oscillation twice as large as the anlytic solution and phase shift 60°. This is the reason why the corrector computation is necessary.

3.3. *Implicit Difference Equations for Corrector Computation*

As discussed in the previous section, the main source of error in larger spacing models is delayed diffusion of fluid. This can be improved by recalculating the fluid velocity field by a corrector method. A corrector procedure may be derived by the use of the implicit difference scheme with the predictor part computed by the explicit difference equations [16]. In the present study, the corrector computation is performed below.

The four sonic characteristic equations (11) with $\alpha = 0$, $\pi/2$, π, and $3\pi/2$ are integrated along the respective implicit characteristic lines shown in Fig. 2. The obtained results are shown below:

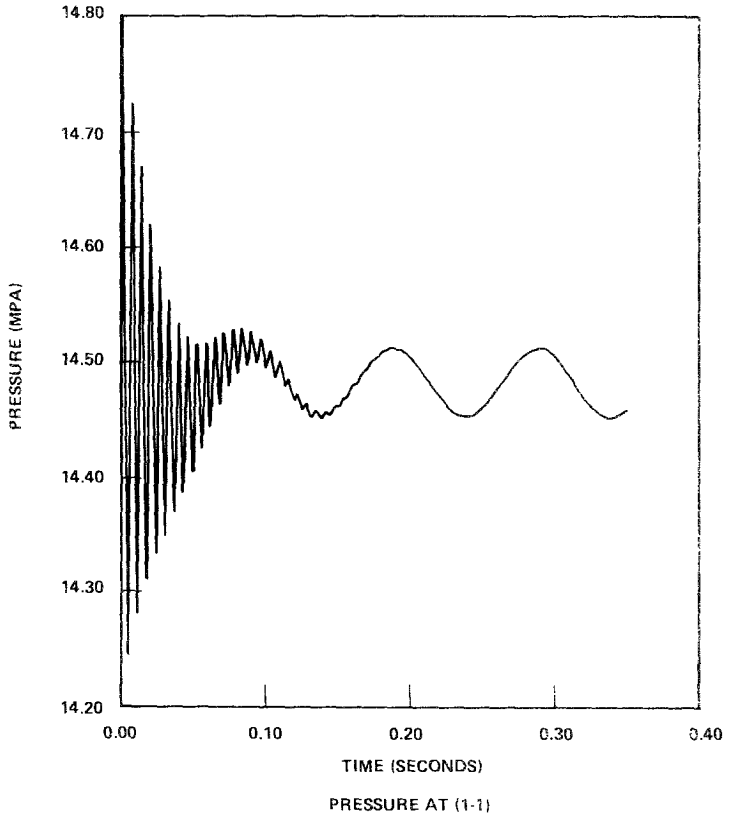

FIG. 10. Pressure history at $x = 0$ of (16 × 5) node model, predictor–corrector computation.

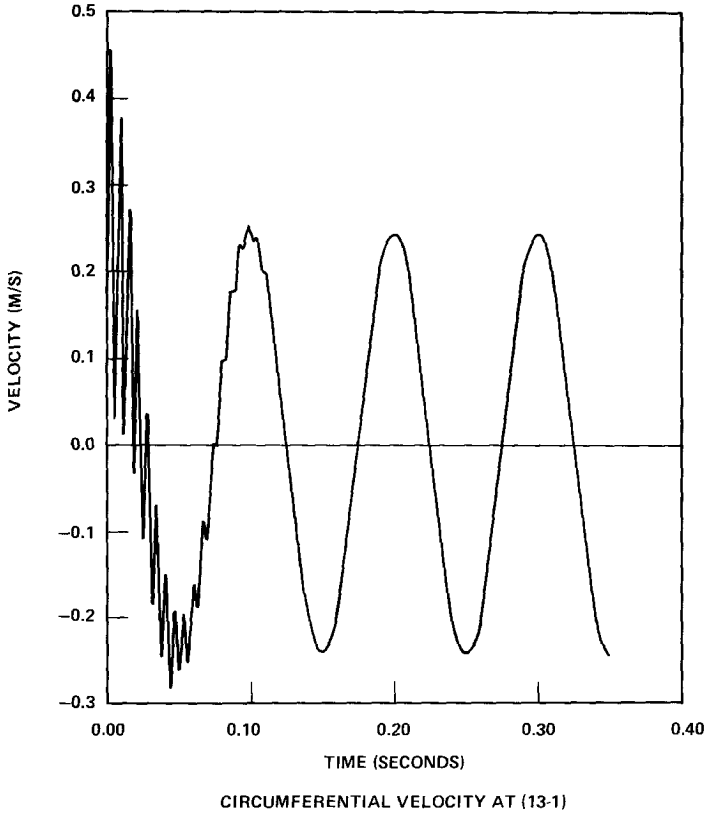

FIG. 11. Velocity history at $x = L/4$ of (16×5) node model, predictor–corrector computation.

$\alpha = 0$ characteristic equation,

$$p_{1+} - p_{0-} - \rho c(u_{1+} - u_{0-}) = -\frac{\Delta t}{2}(\mathscr{G}_{1+} + \mathscr{G}_{10-}) - \rho c^2 \Gamma \frac{\Delta D}{D}; \tag{33}$$

$\alpha = \pi/2$ characteristic equation,

$$p_{2+} - p_{0-} - \rho c(v_{2+} - v_{0-}) = -\frac{\Delta t}{2}(\mathscr{G}_{2+} + \mathscr{G}_{20-}) - \rho c^2 \Gamma \frac{\Delta D}{D}; \tag{34}$$

$\alpha = \pi$ characteristic equation,

$$p_{3+} - p_{0-} + \rho c(u_{3+} - u_{0-}) = -\frac{\Delta t}{2}(\mathscr{G}_{3+} + \mathscr{G}_{30-}) - \rho c^2 \Gamma \frac{\Delta D}{D}; \tag{35}$$

$\alpha = 3\pi/2$ characteristic equation,

$$p_{4+} - p_{0-} + \rho c(v_{4+} - v_{0-}) = -\frac{\Delta t}{2}(\mathscr{G}_{4+} + \mathscr{G}_{40-}) - \rho c^2 \Gamma \frac{\Delta D}{D}. \tag{36}$$

In the above expressions, the quantities with subscripts 1+ through 4+ are those at the current time step and those with 0– are at the previous time step as illustrated in Fig. 2. Now add Eqs. (33) and (35) to get

$$u_{3+} - u_{1+} = -2c\Gamma\frac{\Delta D}{D} - \frac{1}{\rho c}(p_{3+} + p_{1+} - 2p_{0-}) \tag{37}$$

$$-\frac{\Delta t}{2}(\mathscr{G}_{3+} + \mathscr{G}_{1+} - 2\mathscr{G}_{0-})$$

and a similar expression is obtained for the axial fluid flow. The quantities on the right-hand side are computed by the predictor computation of the explicit scheme.

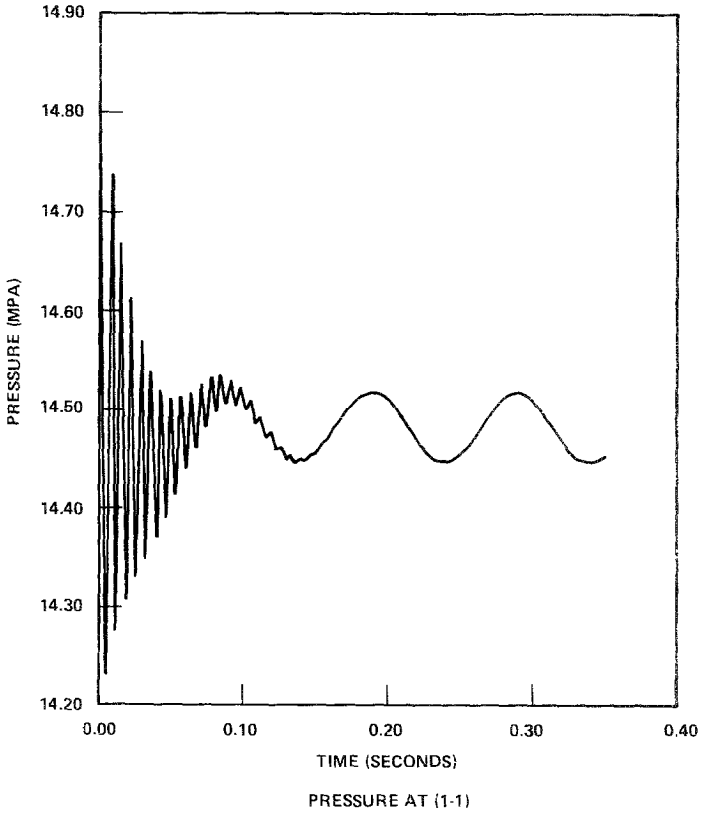

FIG. 12. Pressure history at $x = 0$ of (24×5) node model, predictor–corrector computation.

The flow rates on the left-hand side are related to those at the nodes at the nearest neighbors of point 0+ of (i,j)th node in (x,y) coordinates.

For simplicity, the method of computation is illustrated for the above sample problem. In this example, the axial velocity vanishes and so Eq. (37) is reduced

$$u_0^{(i+1)} - u_0^{(i-1)} = -2\frac{\Delta x}{\Delta t}\Gamma\frac{\Delta D^{(i)}}{D} - \frac{1}{\rho c}(p_0^{(i+1)} + p_0^{(i-1)} - 2p_0^{(i)}) - \frac{2}{\rho c^2}\frac{\Delta x}{\Delta t}(p_0^{(i)} - p_{0-}^{(i)}) \tag{38}$$

or

$$u_0^{(i)} = \frac{1}{2}(u_0^{(i+2)} + u_0^{(i-2)}) + \frac{\Delta x}{\Delta t}\Gamma\left(\frac{\Delta D^{(i+1)}}{D} - \frac{\Delta D^{(i-1)}}{D}\right) + \frac{1}{\rho c}\left[\frac{1}{2}(p_0^{(i+2)} - p_0^{(i-2)}) - (p_0^{(i+1)} - p_0^{(i-1)}) + \frac{\Delta x}{c\,\Delta t}\{p_0^{(i+1)} - p_{0-}^{(i+1)} - (p_0^{(i-1)} - p_{0-}^{(i-1)})\}\right]. \tag{39}$$

In this expression (39), the right hand side is actually computed with the quantities obtained by the predictor computation.

Computed results of the sample problem are shown in Figs. 10–15 for (16×5), (24×5), and (48×5) node models. From these curves the coefficients in Eqs. (26) and (27) are computed and the results are shown in Table II.

The curves of both pressure and velocity histories are almost independent of the size of the node spacings. Comparison of these curves to Figs. 4–9 indicates that the effects of the corrector computation are very large when the spacing is large and the effects almost diminish at (48×5) node model.

To deal with fluid–structure interaction problems, virtual mass method is widely

TABLE II

Coefficients in Eqs. (26) and (27) Due to Predictor–Corrector Computation

Models	Pressure term			Velocity term		
	a_1 (MPa)	a_2 (MPa)	ϕ_p (rad)	b_1 (m/s)	b_2 (m/s)	ϕ_u (rad)
Analytic solution (compressible fluid)	0.370	0.0288	0.	0.241	0.241	0.
(16×5) model	0.321	0.0274	-0.26π	0.247	0.244	0.
(24×5) model	0.352	0.0341	-0.28π	0.244	0.241	0.
(48×5) model	0.397	0.0370	-0.22π	0.259	0.241	0.
Analytic solution (incompressible fluid)	0.0	0.0287	0.	0.0	0.239	0.

used (see, for example, Ref. [17]). This method is equivalent to solving the Laplace equation instead of the wave equation of Eq. (A.6) in Appendix A. The solutions are equivalent to the stationary oscillation terms with frequency ω_0 in Eqs. (A.7), (A.9), and (A.10) at the limit of $C \to \infty$. The computed results are shown in Table II in good agreement with the analytic solution of wave equation because

$$k_0 \gg \omega_0 \tag{40}$$

However, the acoustic oscillations are completely missed in the virtual mass method. The condition of Eq. (40) for validity of virtual mass method, therefore, applies only to the stationary oscillations.

A test problem similar to the above sample problem is previously solved by K-FIX code [8]. The calculated results agree very well with an analytic solution [18] obtained by solving the Navier–Stokes equation for an incompressible fluid. This transient is, of course, the stationary oscillation and the acoustic oscillation does not

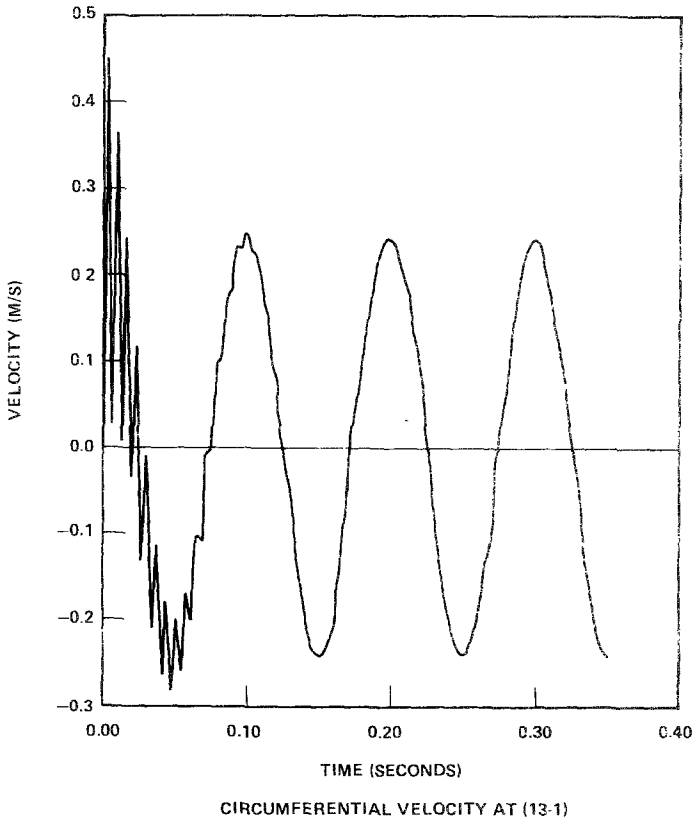

FIG. 13. Velocity history at $x = L/4$ of (24 × 5) node model, predictor–corrector computation.

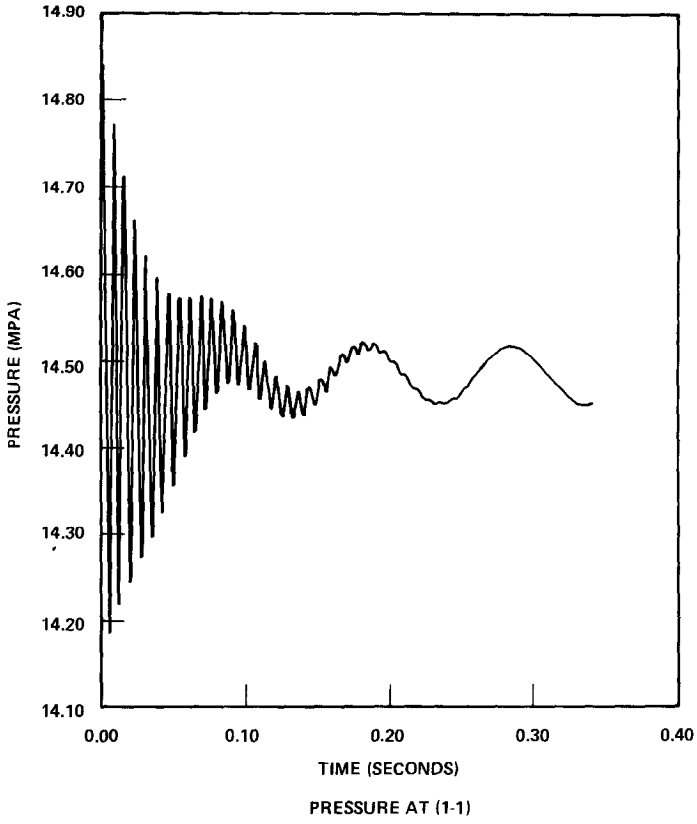

FIG. 14. Pressure history at $x = 0$ of (48×5) node model, predictor–corrector computation.

exist in the analytic solution. Similarly, the transient computed by K-FIX shows no acoustic oscillation. The K-FIX calculation of the stationary pressure oscillation is for an incompressible fluid. The absence of an acoustic oscillation in the K-FIX result is the correct physical consequence of the fluid incompressibility. However, K-FIX seems to yield better results than the present method in computing the stationary pressure oscillation.

4. SUMMARY AND CONCLUSION

In the sample problem, a concentric cyclinder is filled with water and a transient is created by a given sinusoidal oscillation of the inner cylinder. The response of the fluid system is formed of two components, transient oscillation and stationary oscillation. The short-lived transient is due to pressure wave propagation around the

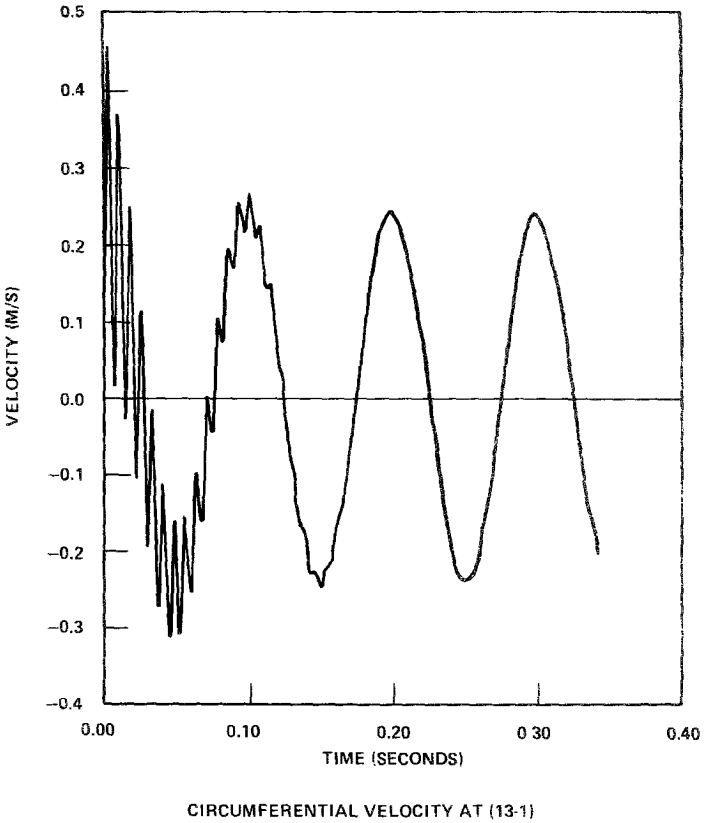

FIG. 15. Velocity history at $x = L/4$ of (48 × 5) node model, predictor–corrector computation.

circumference. After the transient oscillation died out, the stationary oscillation characterized by the frequency of the applied forcing function remains.

This stationary oscillation is the transient previously analyzed by the K-FIX code [8]. It is shown that this part of transient can be accounted for very well by hydrodynamic (virtual) mass method also.

With the explicit method of characteristic, the transient oscillations are computed very well. The difficulty encountered in the stationary part of transient is found to be due to the delayed diffusion of the fluid. Thus, the method of corrector computation is proposed to improve the fluid flow field. With this method, both types of oscillations are demonstrated to be computed fairly well by the method of characteristics.

As discussed in Section 3.2, attainment of balanced fluid flow distribution is very important at every time step: The pressure greatly changes in a control volume due to volume variation or specific volume change because the subcooled water is nearly

incompressible. On the same reason, slight fluid leakage creates a large pressure change. Such a phenomenon is unique to the system of fluid–structure interaction. The numerical solutions in Section 3.3 indeed demonstrate that the corrector computation is important especially to a large spacing model.

Detailed inspection of the computed results reveal some defects of the computation method. The proposed corrector method is not ultimate and it is subject to further improvement in the future. However, the method is good enough to demonstrate the significance of the type of corrector computation for a system of fluid–structure interactions.

In the above sample problem, there is no feedback of hydraulic force field to the structural motion. In the future, the sample problem must be slightly more sophisticated to include such a contribution.

APPENDIX A: ANALYTIC SOLUTION OF THE SAMPLE PROBLEM

The sample problem discussed in Section 3.2 is essentially one-dimensional and it can be solved analytically as follows. The mass conservation relation

$$\frac{\partial}{\partial t}(\rho\, Da\, d\theta) = -\rho\{u(\theta + d\theta) - u(\theta)\}\, D, \tag{A.1}$$

becomes

$$D\frac{\partial \rho}{\partial t} + \rho\Gamma\frac{\partial D}{\partial t} = -\frac{\rho D}{a}\frac{\partial u}{\partial \theta} \tag{A.2}$$

for the annulus gap D varied by the motion of the inner cylinder, where a is the mid-radius of the annulus. The density derivative can be replaced by pressure derivative $d\rho = +(1/c^2)\, dp$ for an isentropic process and so Eq. (A.2) becomes

$$\frac{1}{a}\frac{\partial u}{\partial \theta} + \frac{1}{\rho c^2}\frac{\partial p}{\partial t} = -\Gamma\frac{\dot{D}}{D}. \tag{A.3}$$

By means of the velocity potential ϕ, the fluid velocity is expressed,

$$u = -\frac{1}{a}\frac{\partial \phi}{\partial \theta}. \tag{A.4}$$

Then, momentum conservation relation yields the expression for the pressure,

$$p = p_0 + \rho\frac{\partial \phi}{\partial t}, \tag{A.5}$$

where p_0 is the initial pressure. Applying Eqs. (A.4) and (A.5) to Eq. (A.3), the wave equation with fluid–structure interaction is obtained,

$$\frac{\partial^2\phi}{\partial x^2} - \frac{1}{c^2}\frac{\partial^2\phi}{\partial t^2} = \Gamma\frac{\dot{D}}{D}, \tag{A.6}$$

where $x \equiv a\theta$.
Solutions of Eq. (A.6) are

$$\phi = \frac{\Gamma A\omega_0 c^2}{D_0}\frac{1}{k_0^2 - \omega_0^2}(-\cos k_0 t + \cos\omega_0 t)\cos\frac{2\pi x}{L}, \tag{A.7}$$

where

$$k_0 \equiv \frac{2\pi c}{L}, \tag{A.8}$$

$$u = \frac{\Gamma Ac\omega_0}{D_0}\frac{k_0}{k_0^2 - \omega_0^2}(-\cos k_0 t + \cos\omega_0 t)\sin\frac{2\pi x}{L}, \tag{A.9}$$

$$p = p_0 + \frac{\Gamma A\rho c^2\omega_0}{D_0}\frac{1}{k_0^2 - \omega_0^2}(k_0\sin k_0 t - \omega_0\sin\omega_0 t)\cos\frac{2\pi x}{L}. \tag{A.10}$$

References

1. R. L. Cloud, *in* "Trans. 4th International Conference on SMiRT" F2/4, 1977.
2. H. Lamb, "Hydrodynamics," Dover, New York, 1936.
3. G. Birkhoff, "Hydrodynamics," Dover, New York, 1950.
4. A. Huber and H. Hofmann, *in* "Trans. 4th Int. Conf. on SMiRT," B1/8, 1977.
5. S. Levy and J. P. D. Wilkinson, *in* "Trans., 3rd International Conference on SMiRT," F2/5, 1975.
6. R. G. Dong, *in* "Trans., 5th International Conference on SMiRT," B5/10, 1979.
7. K. Takeuchi, D. J. Kowalski, V. J. Esposito, and F. M. Bordelon, "MULTIFLEX, A FORTRAN-IV Computer Program for Analyzing Thermal-Hydraulic-Structure System Dynamics," WCAP-8709, Westinghouse Electric Corporation, February 1976.
8. W. C. Rivard and M. D. Torrey, "K-FIX: A Computer Program for Transient, Two-Dimensional, Two-Fluid Flow," LASL-Report, LA-NUREG-6623, Suppl. II, 1978.
9. F. Katz and E. G. Schlechtendahl, *in* "Trans., 5th International Conference on SMiRT," B6/6, 1979.
10. J. K. Dienes, C. W. Hirt, and L. R. Stein, "Multi-Dimensional Fluid–Structure Interactions in a Pressurized Water Reactor," pp. 15–34, ASME Publications, AMD-Vol. 26, ASME, New York 1977.
11. K. Takeuchi, *Nuclear Technology* **39** (1978), 155–166.
12. A. L. Florence and G. R. Abramson, "Simulation of a Hypothetical Core Disruptive Accident in a Fast Flux Testing Facility," HEDL-SRI-1, Hanford Engineering Development Laboratory, 1973.
13. T. Grillenberger and B. Oesterle, *in* "Trans., 4th Int. Conf. on SMiRT," B2/5, 1977.
14. E. G. Schlechtendahl, *Nuclear Safety* **20** (1979), 551–563.

15. A. C. SPENCER, *in* "Proc. ANS Topical Meeting Mathematical Models and Computational Techniques for Analysis of Nuclear Systems," Ann Arbor, Mich. April 1973.
16. L. FOX, "Numerical Solution of Ordinary and Partial Differential Equations," Pergammon, London, 1962.
17. R. G. DONG, "Effective Mass and Damping of Submerged Structures," UCRL-52342, Lawrence Livermore Laboratory, 1978.
18. C. BRENNEN, *J. Fluid Mech.* **75** (1976), 173–179.
19. K. TAKEUCHI AND A. W. GURCAK, JR., *Trans. Amer. Nuclear Soc.* **21** (1975), 199–200.